Age of the Canada Basin, Arctic Ocean: Indications From High-Resolution Magnetic Data

Tao Zhang, J. Dyment, Jinyao Gao

Age of the Canada Basin, Arctic Ocean: Indications From High-Resolution Magnetic Data

Tao Zhang[1,2], Jérôme Dyment[3], and Jinyao Gao[1,2]

[1]Key Laboratory of Submarine Geosciences, State Oceanic Administration, Hangzhou 310012, China.

[2]Second Institute of Oceanography, Ministry of Natural Resources, Hangzhou 310012, China.

[3]Institut de physique du globe de Paris, Université de Paris, CNRS, F-75005 Paris, France.

Key Points:

- High-resolution deep-tow and sea surface magnetic data in the ice-covered Canada Basin of the Arctic are presented.
- The crustal age of the Canada Basin is 139.5-128.6 Ma (142.4-132.8 Ma), with a spreading rate of ~32 (38) mm/yr.
- The opening of the Canada Basin was roughly contemporaneous with the closure of the ancient South Anyui Ocean.

Abstract: The origin and history of the Amerasia basin are long-running debates, which hinder our knowledge of the Mesozoic tectonic configurations and geodynamic processes in the Arctic. This lack of knowledge is due in part to the paucity of accurate magnetic data in the ice-covered basin. Here, we identify the crustal age of the Canada Basin, a major part of the Amerasia Basin, through high-resolution deep-tow and sea surface magnetic data. The best fit of the four pairs of magnetic lineations revealed by the high-resolution magnetic data is 139.5-128.6 Ma (or 142.4-132.8 Ma, depending on the geomagnetic polarity timescale). The crustal age provides crucial constraints on the evolution of the circum-Arctic tectonic features and generally supports the hypothesis that the opening of the Amerasia Basin is related to the subductions during the closure of the South Anyui Ocean.

Plain Language Summary

The Amerasia Basin of the Arctic Ocean is one of the last major puzzles of the plate reconstructions, due to the lack of age knowledge. The identification of magnetic anomalies is the routine method of acquiring the age of oceanic crust, yet floating ice in the basin makes it difficult to obtain magnetic data. We collected deep-tow magnetic data in the basin by lowering a magnetic sensor to a depth of ~2000 m, which provides high-resolution data and avoids floating ice. The identified magnetic lineations indicate the Amerasia Basin opened at 139.5-128.6 Ma (or 142.4-132.8 Ma, depending on the geomagnetic polarity timescale). The contemporaneous closure of the ancient South Anyui Ocean (~1000 km in the south) may have provided space for the opening of the Amerasia Basin. This interpretation then generally supports the existing hypothesis that the opening of the Amerasian Basin is associated with the subduction process in the South Anyui Ocean. Nevertheless, a more sophisticated geodynamical model is still needed.

1 Introduction

The opening of the Amerasia Basin shaped the Mesozoic configuration of major circum-Arctic geological features such as Arctic Alaska, Chukotka, and Arctic Canada. A robust tectonic model of the Amerasia Basin would yield insights into Arctic paleogeography, paleoclimate, the driving forces of the opening of the basin, and resource exploration within the dozens of circum-Arctic sedimentary basins [*Shephard et al.,* 2013]. However, the nature and age of the Amerasia Basin have been debated for decades [e.g.,*Embry,* 1990, 2000; *Grantz et al.,* 1998, 2011; *Lane,* 1997; *Miller et al.,* 2006,2017]. Recently, the oceanic nature of the crust in the Canada Basin, which forms the major part of the Amerasia Basin, was revealed by refraction seismic data [*Chian et al.,* 2016]. The roughly symmetric oceanic lithosphere about a N-S trending gravity low indicates that the Canada Basin was an E-W spreading oceanic basin. Nevertheless, the age of the Canada Basin remains elusive, with an inferred range of 160-72 Ma from investigations on the stratigraphy and volcanism along its margins and sparse geophysical data in the basin [e.g., *Alvey et al.,* 2008; *Chian et al.,* 2016; *Døssing et al.,* 2013; *Embry,*1990; *Gaina et al.,* 2014; *Grantz et al.,* 2011; *Lane,*1997; *Langseth* et al., 1990; *Miller et al.,* 2006, 2017; *Taylor et al.,* 1981]. In particular, the low-resolution airborne magnetic data in the basin with an exceptionally thick (4-11 km) sedimentary cover impede the definitive identification of crustal age with magnetic anomalies. In this paper, we present recently sampled, high-resolution, deep-tow and sea surface magnetic data in the ice-covered Canada

Basin (Figure 1). We identify the crustal age of the Canada Basin through the amplitude, shape, and pairs of the magnetic lineations. We discuss the relationships between seafloor spreading of the Canada Basin and regional unconformities along the margins of the Canada Basin. We further suggest that the opening of the Canada Basin may be kinematically and geodynamically related to the demise of the South Anyui Ocean, which partly supports the existing models [e.g., *Koulakov et al.,* 2013; *Kuzmichev*, 2009].

2 Geological Settings

Located at the center of the Arctic region, the Amerasia Basin is bounded by Arctic Alaska, Chukotka, East Siberian Shelf, Lomonosov Ridge, and Arctic Canada (Figure 1). Numerous models have been proposed to explain the formation of the Amerasia Basin [e.g., *Lawver and Scotese,* 1990; and references therein]. The floating ice, thick sediment, and presence of the High Arctic Large Igneous Province make it difficult to validate those models. Among them, the generally accepted anticlockwise rotation model proposes that the Chukotka-Alaska region rotated from Arctic Canada with a pole of rotation located near the Mackenzie Delta in Early Cretaceous [*Carey,* 1955; *Embry,* 1990, 2000; *Embry and Dixon,* 1990; *Grantz et al.,* 1998, 2011; *Halgedahl and Jarrard,* 1987; *Mickey et al.,* 2002]. Recent seismic [*Chian et al.,* 2016] and potential field data [*Andersen et al.*, 2010; *Gaina et al.*, 2011] from the Canada Basin revealed that the oceanic crust is roughly symmetrical about the N-S trending relict axis shown by a linear gravity low. The extent of oceanic crust and location of the relict axis are broadly consistent with the depictions in the rotation model. However, this model is challenged by alternative models [e.g., *Chian et al.,* 2016; *Døssing et al.,* 2018; *Hutchinson et al.,* 2017; *Koulakov et al.,* 2013; *Lane,* 199], in part due to the uncertain age of the Amerasia Basin.

In the anticlockwise rotation model, the Amerasia Basin opened in two stages [e.g., *Grantz et al.,* 2011]. The age of initial rifting ranges from the Early Jurassic (Hettangian) [*Hubbard et al.,* 1987] to early Middle Jurassic (Aalenian) [*Embry and Dixon,* 1990; *Mickey et al.,* 2002]. The second stage or main stage of opening is no older than Oxfordian-Tithonian (158-145.5), supported by the synrift sequence onlapping late Oxfordian-Tithonian strata at the Northwind Ridge [*Grantz et al.,* 1998]. Nevertheless, the age of seafloor spreading is still highly controversial. *Grantz et al.*[2011] proposed that seafloor spreading was initiated in Hauterivian (~131 Ma) after correlating the beds of the late synrift sequences to the widely distributed Lower Cretaceous unconformity. *Halgedahl and Jarrard* [1987] suggested that the Alaskan North Slope was still adjacent to the Arctic Islands in Valanginian based on the paleomagnetic data from the North Slope Kuparuk Formation. *Embry and Dixon* [1990] interpreted the Albian-Cenomanian unconformity in the Sverdrup Basin as the breakup unconformity. Based on a petrologic study, *Miller et al.* [2017] suggested that spreading in the Amerasia Basin may have ended at ~90 Ma.

Several interpretations of the magnetic anomaly have been proposed in the Canada Basin based on available low-resolution airborne magnetic data. However, the low amplitude and limited two pairs of conjugate positive magnetic anomalies made any oceanic crustal age identification uncertain and unreliable [*Chian et al.,* 2016; *Gaina et al.,* 2014; *Grantz et al.,* 2011; *Taylor et al.,* 1981]. *Taylor et al.* [1981] tentatively suggested that the crustal age of the Canada Basin ranges from the earliest Late Jurassic to Valanginian (CM25-CM12, 160-136 Ma). *Grantz et al.* [2011] and *Chian et al.* [2016] proposed similar identifications of chrons CM4n to CM2n (131-127.5 Ma), with a spreading rate up to 75 mm/yr. *Gaina et al.* [2014] identified CM16-CM4 (137.8-126.5 Ma) according to Channell (1995) and found a spreading rate of ~30 mm/yr for the younger stage of seafloor spreading in the northern part of the Canada Basin.

The morphology of the rift valley offers an independent constraint on the spreading rate of the Canada Basin. Reflection seismic data indicate that the valley of the relict ridge axis has depths of 1.0-1.5 km and widths of 30-40 km [*Chian et al.,* 2016; *Grantz et al.,* 2011], which is typical for a slow spreading (< 75 mm/yr) ridge axis. The rough basement relief and relative thin crust (4-7 km) [*Chian et al.,* 2016] are also consistent with the characteristics of the slow to ultraslow spreading ridges [*Dick et al.,* 2003; *Malinverno,* 1991].

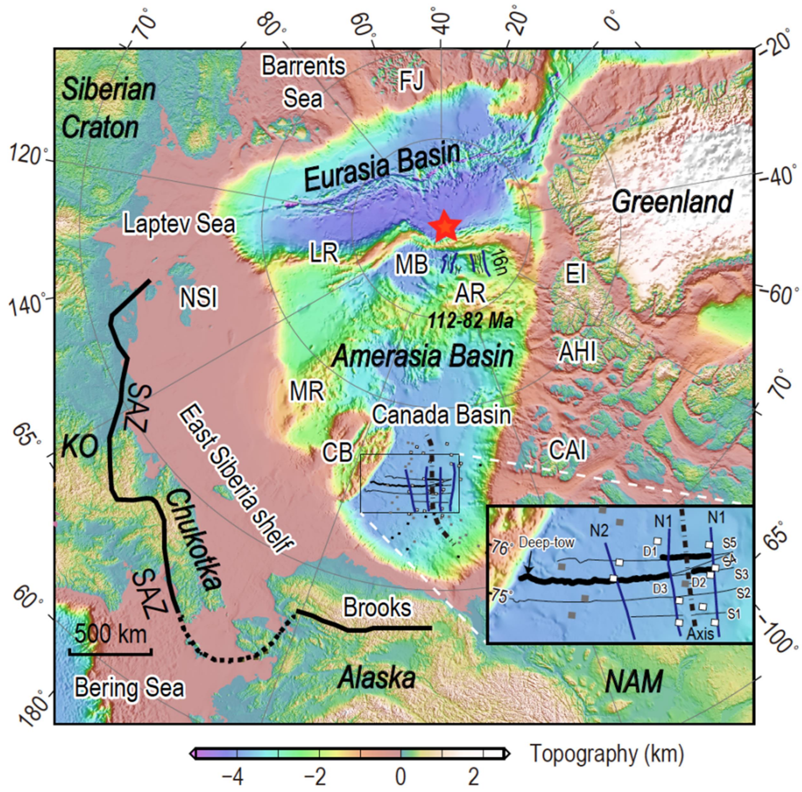

Figure 1. Topography of the Circum-Arctic Region. The location of SAZ is from *Shephard et al.* [2013]. The location of the survey lines, relict ridge axis, and broad magnetic highs (N1 and N2) are shown in the inset. AHI = Axel Heiberg Island; AR = Alpha Ridge; CAI = Canadian Arctic Islands; CB = Chukchi Borderland; EI = Ellesmere Island; FJ = Franz Josef Land; KO = Kolyma-Omolon; LR = Lomonosov Ridge; MB = Makarov Basin; MR = Mendeleev Ridge; NAM = North American craton; NSI = New Siberian Islands; SAZ = South Anyui suture Zone.

3 Data acquisition and processing

We use one deep-tow magnetic profile (consisting of three sections D1-D3) and five sea surface magnetic profiles (S1-S5) at75°-76°N collected by Icebreaker "Xue Long" in 2014 and 2016 to 2017, respectively (Figure 1). Most profiles are perpendicular to the N-S trending gravity anomaly low near 142°W. In the summer of 2014, ~500 km deep-tow magnetic data were sampled by a MarineMagnetics™ Overhauser magnetometer with a sensitivity of 0.015 nT mounted on a titanium-alloy frame and towed ~1.3 km above the seafloor at a speed of 2-3 knots (supporting information Figure S1). To measure the depth of the frame, a pressure sensor Sea-Bird™ SBE was mounted on the wire at 5 m above the frame. Controlled by the payoff of the winch, the depth of the magnetic sensor is ~2.5 km in average and varies within a relatively limited range of ~±0.5 km (Figure S1).

The deep-tow magnetic data are processed with the following five steps. (1) Magnetic data are merged with GPS position data and sensor depth data (Figure S1). (2) The International Geomagnetic Reference Field (IGRF) [*Thébault et al.,* 2015] is removed. (3) The diurnal variations are removed. (4) The data are resampled to equally spaced (50 m) points. (5) A Fourier transform method is used to upward-continue the data from an uneven level to a constant depth of 2 km below sea surface [*Guspi,* 1987]. Among these steps, steps 1, 2, and 4 have little effect on the characteristics of magnetic data. For step 3, we use the magnetic variations recorded at the Barrow and Resolution Bay magnetic observatories. Since the survey area is approximately one-fourth between the two observatories, we use a weighted average of Barrow (3/4) and Resolution Bay (1/4) magnetic data for the diurnal correction. During collection of the deep-tow magnetic data, the daily magnetic variation had amplitudes up to ±100 nT (Figures S2 and 2), with a standard deviation of 40.8 nT. The daily magnetic variation is smaller but comparable to the collected magnetic data with amplitudes up to 400 nT and an STD of 85.8 nT (Figure S2). We remove all data with diurnal variation exceeding ±50 nT, although the deep-tow magnetic data are probably much less affected by the ionospheric noise since this noise is attenuated by the conductive sea water above [*Miller,* 1977]. After the diurnal correction, the upward-continued magnetic anomaly to sea level fits well with the sea surface magnetic anomaly along the same track collected in 2016 (Figure 2), indicating that the diurnal correction efficiently reduce the associated external magnetic variations. In step 5, we remove the signals with wavelengths longer than 100 km or shorter than 2 km and upward-continued the magnetic data to 2 km below the sea surface, to obtain the deep-tow magnetic anomaly ~2 km above the sea floor and ~7.5 km above the igneous crust [*Mosher and Hutchinson,*2019].

Along the deep-tow magnetic survey in 2014, most tracks (> 60%) were covered by floating ice. Nevertheless, in the areas with light ice-conditions, we collected ~110 km of sea surface magnetic data with a Cesium magnetometer towed 450 m behind the *R/V* “Xue Long”. In 2016 and 2017, the ice conditions were rather light (~20% ice coverage), which allowed us to collect ~1400 km of sea surface magnetic data. The associated International Geomagnetic Reference Field model [*Thébault et al.,* 2015] and the diurnal variations are also removed from the sea surface magnetic data (Figure S2). For comparison, we also include the airborne magnetic anomaly data of *Taylor et al.* [1981] in Figure 2.

4 Data presentation

Two paired coherent broad magnetic highs are observed by the deep-tow, sea surface, and airborne magnetic data (Figure 2). Here, we name them normal 1 (N1) and normal 2 (N2) anomalies for the broad magnetic high close to and away from the relict ridge axis, respectively. On the western flank, N1 with peak-to-trough amplitudes of 150-200 nT straddles 50-80 km in the sea surface magnetic data. N2 on the western flank has larger amplitudes (up to 300 nT) and broader widths (90-120 km) than N1. The amplitudes of N1 and N2 are comparable to the magnetic signals observed at other slow to ultraslow spreading ridges [e.g.,*Gee and Kent,* 2007]. The two paired broad magnetic highs are roughly symmetrical with respect to the fossil axis, suggesting that these magnetic anomalies may reflect geomagnetic reversals and seafloor spreading in the Canada Basin. In addition, the power spectrum analysis of the deep-tow magnetic data and surface magnetic data suggests that the magnetic source layer is situated~10 km below the sea surface and then resides within the igneous crust (Figure S3). Furthermore, the magnetic lineations are independent of the gravity anomalies (Figure S4), which further implies that the magnetic lineations are not associated with variations in the lithospheric structure. Therefore, the paired magnetic lineations (N1 and N2) reflect spatial variations in crustal magnetization associated with the record of magnetic field reversals within the oceanic crust.

Two pairs of magnetic anomalies are not sufficient for a unique, unambiguous correlation with the geomagnetic polarity time scale (GPTS). In addition to N1 and

N2, some previously undetected, spatially coherent, low amplitudes and short-wavelength magnetic anomalies are also observed in the high-resolution deep-tow magnetic data and to a lesser extent in the sea surface magnetic data (Figure 2). Such small magnetic anomalies could be related either to short geomagnetic polarity intervals, excursions (i.e. aborted reversals) or paleointensity variations, which would all be recorded in a similar way on both side of the (now fossil) ridge axis, or by crustal tectonic processes, short-period external magnetic field fluctuations, and/or artifacts during the data acquisition, which may have a different distribution. Among them, two short-wavelength low-amplitude magnetic anomalies could be ascribed to the geomagnetic variations, more likely to field reversals, considering their repeatability and consistency between profiles and their presence on both flanks of the relict ridge. Near the center of the broad magnetic low intervening N1 and N2 on the western flank, a narrow magnetic high with an amplitude of ~200 nT is observed on the deep-tow magnetic profile (Figure 2). The amplitude of this anomaly decreases to ~50-100 nT on the sea surface magnetic profiles. On the conjugate eastern flank, a similar magnetic high is also present along three of the five sea surface profiles. Thus, this magnetic high may be ascribed to a short normal polarity interval in a relatively long period dominated by reversed polarities and is termed small normal anomaly 1 (SN1). Besides, a magnetic low with an amplitude of ~30 nT is observed near the center of N1 on the deep-tow magnetic anomaly on the eastern flank (Figure 2c). This magnetic low is also observed on almost all sea surface magnetic profiles on the eastern flank of the ridge axis, except on profileS5. The consistency between profiles on the eastern flank suggests that this magnetic low is associated with one or a series of short reversed polarity intervals (termed SR1) in a relatively long period dominated by normal polarity.

Encouraged by the consistency of the magnetic anomalies between profiles and on conjugate flanks, we stack all the sea surface data and the upward-continued deep-tow data to the sea surface in an attempt to enhance the signal/noise ratio and better characterize the magnetic anomalies (Figure 2f). We also stack the airborne magnetic data by correlating N1 and N2 between these profiles (Figure 2f). Both stacked data show that N2 has higher amplitude than N1 on both flanks of the fossil ridge. We then identify the crustal age by fitting the observed anomaly and stacked anomaly with synthetic magnetic anomalies computed from GPTSs.

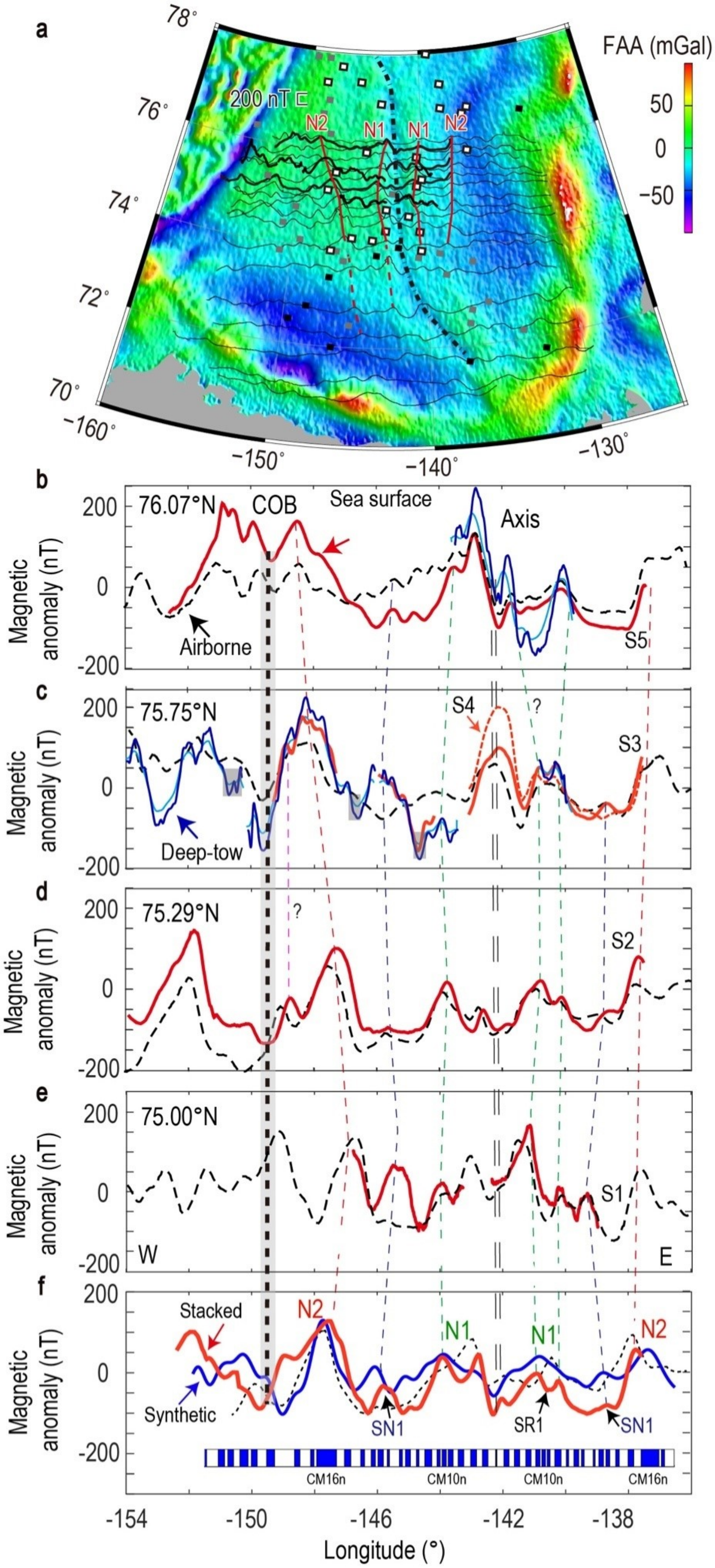

Figure2. Deep-tow and sea surface magnetic anomalies in the Canada Basin. (a) Deep-tow, sea

surface, and airborne magnetic anomalies along their tracks. The background is based on the satellite-derived free air anomaly data [*Sandwell et al.* 2014]. The continental, transitional, and oceanic crust identified from sonobuoy data [*Chian et al.,* 2016] are shown in black, gray, and white squares, respectively. The relict ridge axis is marked with a dashed line. (b-e) Deep-tow, sea surface, and airborne magnetic anomalies at different latitudes. The upward continued deep-tow data to sea surface and to 2000 m below sea surface are shown in light blue and blue, respectively. The sea surface and airborne magnetic data are shown in red and black, respectively. The data associated with diurnal variation > 50 nT are marked with gray boxes. The profiles S2-S5 and profile S1 are collected in 2016 and 2017, respectively. No reduction to the pole is necessary, as the data are collected at high latitude. (f) Stacked sea surface (red), stacked airborne (black), and best-fitting synthetic (blue) magnetic anomalies. The consistent magnetic anomalies between profiles are linked with dashed lines. The magnetic bodies in MHTC12 [*Malinverno et al.,* 2012] that produce the synthetic magnetic anomaly at the depth of basement are also shown. For more information on the correlation between the stacked magnetic anomaly and synthetic magnetic anomalies, see the text and Figures S5-S6.

5 Identification of magnetic anomalies

Based on the onshore and along-margin geological evidences, the age of the Canada Basin is not older than the Late Jurassic (~160 Ma) and not younger than the Late Cretaceous (~72 Ma) [e.g., *Embry,* 1990; *Gaina et al.,* 2014 ; *Grantz et al.,* 2011 ; *Miller et al.,* 2006, 2017 ; *Taylor et al.,* 1981]. Since the deep-tow magnetic anomalies are rather strong (up to 400 nT) and well-marked, we do not expect that they formed during the so-called “Jurassic quiet zone” (>157 Ma) characterized by numerous polarity reversals and a weak geomagnetic intensity, or during the Cretaceous quiet zone (~120.6 (124)-83 Ma) characterized by a constant (or very dominant) normal polarity [*Granot et al.,* 2012]. Neither the relatively long polarity intervals of chrons C32n-C33n nor the intervening excursions or intensity variations (the "tiny wiggles" depicted by *Bouligand et al.* [2006]) produce the observed magnetic features. We therefore restrict our investigations and compare the observed and stacked anomalies with synthetic anomalies generated using the M-Series GPTS between the Jurassic quiet zone and the Cretaceous quiet zone.

The positions of the continent-ocean boundaries on both flanks of the relict ridge axis are derived from the sonobuoy data (Figure 1) [*Chian et al.,* 2016]. The location of the relict ridge axis is indicated by the ~15 mGal N-S trending gravity low at~142°W. We select the upper boundary of layer 2 (igneous basement) from the sonobuoy data as the upper limit of the magnetic source [*Chian et al.,* 2018; *Mosher and Hutchinson,* 2019]. To produce sea surface anomalies with amplitudes up to 300 nT at ~9.5 km above the magnetic sources, the thickness and magnetization of the magnetic sources are assumed to be 1 km and 5 A/m, respectively. The mean paleolatitude (72°N) of the magnetized bodies is based on the paleolatitude (~68°-76°N) of the Alaskan North Slope between 120 Ma and 150 Ma [*Seton et al.,* 2012]. Since there are still controversies about the age of CM0r, we adopt two GPTSs, MHTC12 [*Malinverno et al.,* 2012] for which the age of CM0r is ~120.6 Ma, and GTS2012 [*Ogg,* 2012] for which it is ~125 Ma, to compute synthetic magnetic anomalies (Figures S5 and S6).

We adopt both the cross-correlation [*DeMets et al.,* 2010] and visual inspection methods to determine the best-fitting polarity reversal sequences (Figures S5 and S6). Based on the least-square fitting criteria, the cross-correlation method quantitatively compares the amplitude and shape of the part of the stacked magnetic anomalies between the two broad magnetic highs (N1 and N2) with synthetic data (Figure S5). In visual inspection method, we fit N1, N2, SN1, and SR1 of the observed data with the synthetic magnetic anomalies.

Both methods give similar results: The synthetic data produced by the CM7r-CM16n (CM17n?) sequences for both GPTSs are the best fit of the stacked data (Figures 2f and S6). A series of normal polarity intervals of CM9n-11n and the long CM16n produce N1 and N2, respectively. The CM13n and negative polarity intervals between CM9 and CM11 are associated with the low-amplitude magnetic high (SN1) intervening N1 and N2 and the low-amplitude magnetic low (SR1) near the center of N1, respectively.

Therefore, the crustal age of the Canada Basin could be 139.5-128.6 Ma (142.4-132.8 Ma) according to the MHTC12 (GTS2012), and seafloor spreading occurred between Berriasian and Early Hauterivian (Figure S6). Near 75°N, the associated full spreading rate was~32 (38) mm/year at the beginning of spreading and slowed down to ~30 (30) mm/year in the last ~3 Ma before the cessation. Seafloor spreading is slightly asymmetrical, with rates 5% faster on the western flank. Since the distance between the lineations N2 on both flank is slightly larger in the north than in the south (Figure 2a), the average spreading rates at the northern (~76.5°N) and southern (~74°N) limits of N2 are inferred to be 34.5 (39.0) and 28.3 (31.9) mm/year, respectively. The slow spreading rate is consistent with the presence of the ~1.5 km-deep rift valley and the 4-6 km thin crust in the Canada Basin. Since there are no robust constraints such as fracture zones on the spreading direction, we calculate the spreading rate assuming an orthogonal spreading. Recently, opening models of the Amerasia Basin involving a strike-slip component (oblique spreading or transtensional deformation) have been proposed based on northeast-treading structural fabrics [*Døssing et al.,* 2018; *Hutchinson et al.,* 2017]. The highly oblique spreading (up to ~50°) requires a spreading rate ~1.5 times faster than that estimated from the magnetic lineations. In this case, the spreading rate we estimated corresponds to the effective spreading rate termed by *Dick et al.* [2003] and still matches the deep rift valley and thin crust in the Amerasia Basin. Among numerous proposed crustal ages from magnetic data, our result agrees better with the crustal age of 137.8-126.5 Ma proposed by *Gaina et al.* [2014]. As the seismic reflection data show that the synrift sequences overlap late Oxfordian-Tithonian (~158-145.5 Ma) marine shelf or shelf basin deposits in three piston cores on the Northwind Ridge [*Grantz et al.,* 1998, 2011], we further infer that the main stage of opening of the Canada Basin may had been fulfilled by rifting from late Oxfordian-Tithonian to Berriasian and the consequent seafloor spreading until early Hauterivian.

6 Discussion

Three main regional unconformities (late Callovian-early Oxfordian, late

Hauterivian, and mid-Aptian) were interpreted as the breakup unconformity and were used to date the initial seafloor spreading of the Canada Basin by various authors [*Embry and Dixon,* 1990; *Grantz et al.,* 2011; *Grantz and May,* 1982; *Hubbard et al.,* 1987]. However, the seafloor spreading during Berriasian-early Hauterivian of the Canada Basin suggests that the relationships between those regional unconformities along the margins and the initiation of seafloor spreading in the Amerasia Basin cannot be steadily associated. The thinned continental crust and transitional crust in the Canada Basin could be as wide as 300 km [*Chian et al.,* 2016]. During the formation of such wide margins, sequential active faulting may have migrated toward the future oceanic crust [*Brune et al.,* 2014]. Therefore, further evidences, such as the reflection seismic data from the Canada Basin to the areas of the regional unconformities, are needed to address the relationship between the regional unconformities and the breakup event. Even so, part of the rifted margins of the Canada Basin were already subaquatic at the time of the breakup [*Grantz et al.,* 2011], which may further obscure the identification of the breakup unconformity [Franke, 2013].

The crustal age of the Canada Basin also provides further kinematic and geodynamic implications for the Mesozoic circum-Arctic region. Between Late Jurassic and Early Cretaceous, the Arctic Alaska and Chukotka blocks experienced intense tectonic activity, including collision between the Alaska- Chukotka and the Kolyma-Omolon blocks to the south, the associated closure of the South Anyui Ocean

(SAO), and the closure of the Angayucham Ocean (Figure 3). The subductions that consumed the SAO have been postulated as the source of driving force for the opening of the Amerasia Basin based on tomography images [e.g., *Gaina et al.,* 2014; *Koulakov et al.,* 2013] and the range of South Anyui suture zone [*Kuzmichev*, 2009]. Our results further show that the opening of the Canada Basin was roughly contemporaneous with the closure of the SAO and the associated subductions. At the beginning of the main rifting stage of the Canada Basin (~158 Ma), the closure of SAO was initiated by southward and northward subductions (Figure 3a), as indicated by the ages of the Oloy Arc (~160–140 Ma) in the south and the Nutesyn Arc (~160–150 Ma) in the north, respectively [*Amato et al.,* 2015; *Layer et al.,* 2001; *Shephard et al.,* 2013]. The final stage of the closure of the SAO was fulfilled by the collision between the Chukotka and Kolyma-Omolon blocks. Although the collision mainly occurred between 119 and 106 Ma [*Amato et al.,* 2015; *Miller et al.,* 2009; *Sokolov et al.,* 2002, 2009], it may started as early as 130–124 Ma [*Layer et al.,* 2001; *Toro et al.,* 2003], which also coincide with the cessation of the seafloor spreading in the Canada Basin at 128.6 Ma. This temporal and spatial consistency lead us to suggest that the closure of the SAO provided space for the opening of the Canada Basin, and the collision between the Chukotka and Kolyma-Omolon blocks at the final stage of the SAO closure terminated the seafloor spreading of the Canada Basin. This inference then generally supports the idea that the opening of the Canada Basin is associated with the subduction process in the SAO [*Koulakov et al.,* 2013;

Kuzmichev, 2009]. Nevertheless, the clockwise rotation of the "Arctida" plate requires an overall higher opening rate in the southern part of the Canada Basin [*Koulakov et al.,* 2013]. As "a common back-arc basin" proposed by *Kuzmichev* [2009], the Canada Basin was also too far away (more than 1,000 km) from the subduction zones in the SAO, since a back-arc spreading center is usually limited to a distance of 200–300 km from a trench [e.g., *Toksöz & Hsui,* 1978[. Further information on the geometry, extent, and polarity reversals of the subductions in the SAO may help to refine a more comprehensive geodynamic model to address these issues.

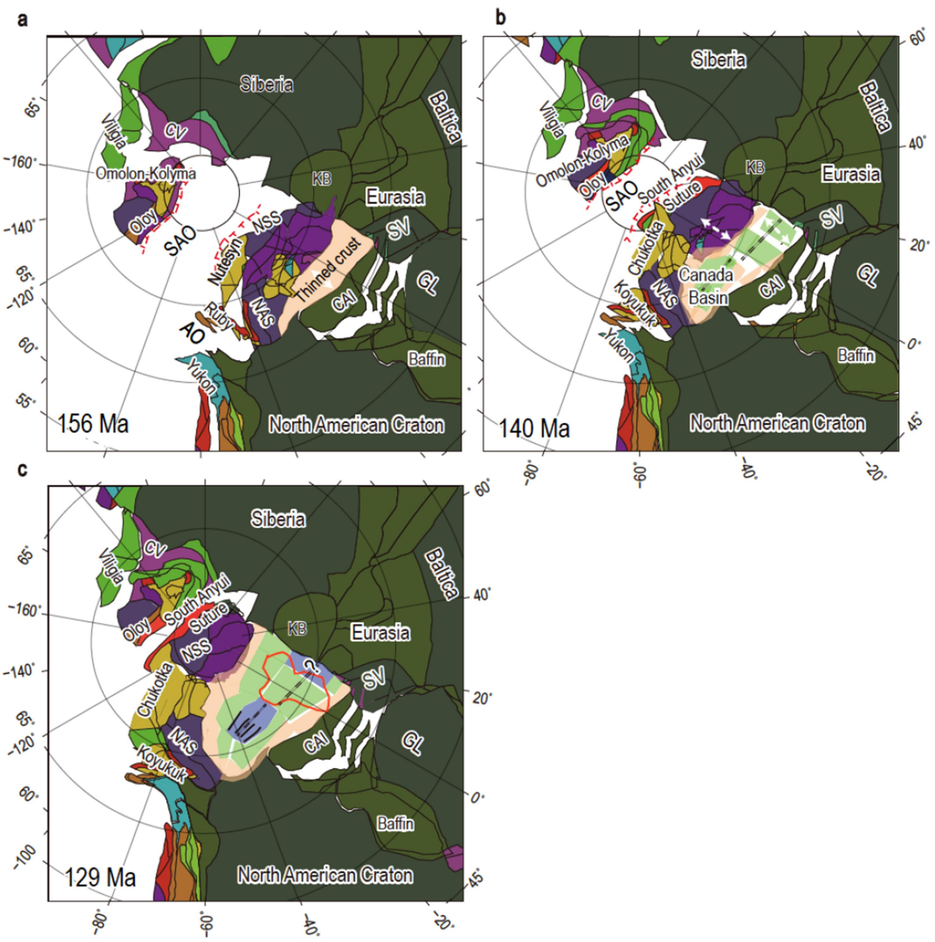

Figure3. Plate reconstructions of the circum-Arctic Region between 156 Ma and 129 Ma. The shapes of the geological features are based on *Müller et al.* [2016]. (a) Rifting created the

Amerasia Basin. The South Anyui Ocean was then subducting to the south and north. East of the SAO, the Angayucham Ocean (AO) and associated Koyukuk Arc (initiated at ~160-145 Ma) are believed to be the eastern extensions or the counterparts of the SAO and Nutesyn Arc [*Amato*, 2004, 2015; *Churkin et al.,* 1981; *Nokleberg et al.,* 2000], respectively. (b) Initial seafloor spreading in the Amerasia Basin. (c) Seafloor spreading cessation in the Amerasia Basin. The position of the future Alpha Ridge is marked by a red line. Since the position and geometry of the Chukchi Borderland in Mesozoic remain controversial [*Grantz et al.,* 1998; *Hutchinson et al.,* 2017; *Miller et al.,* 2006], we only place the CBL in (c) according to its present configuration. The rifting direction in strike-slip models is shown in dashed arrow along the eastern boundary of the Northwind Ridge [*Døssing et al.,* 2018; *Hutchinson et al.,* 2017]. Note the northeast-trending strike slip is subparallel to the subduction zones in the SAO, which may require a new explanation about the dynamic relationship between them. The inferred thinned continental crust, transitional crust, and oceanic crust in the Canada Basin are marked with brown, green, and blue, respectively. CBL = Chukchi Borderland; CV = Central Verkhoyansk; GL = Greenland; KB = Kara Block; NAS = North Alaska Slope; NSS = Northern Siberia Shelf; SAO =South Anyui Ocean; SV = Svalbard.

Acknowledgments

The authors thank the captain Quan Shen and all the crews of the R/V “Xue Long”. We benefit from discussion with Min Ding, Weiwei Ding, and Zhaocai Wu. We are grateful to Carmen Gaina and an anonymous reviewer, whose thorough reviews have greatly improved the manuscript. This work is supported by the National Natural Science Foundation of China (grant 41576065), the Scientific Research Fund of the Second Institute of Oceanography, SOA (grant QNYC201503), and the Chinese Polar Environment Comprehensive Investigation and Assessment Programs (grant CHINARE03-03). There is no financial conflict of interest for any author. The magnetic data is available at https://github.com/yangchunguo/ DataCiteRepository.

References

Alvey, A., C. Gaina, N. Kusznir, and T. Torsvik (2008), Integrated crustal thickness mapping and plate reconstructions for the high Arctic, *Earth and Planetary Science Letters,* 274(3-4), 310-321. https://doi.org/10.1016/j.epsl.2008.07.036

Amato, J. M., J. Toro, V. V. Akinin, B. A. Hampton, A. S. Salnikov, and M. I. Tuchkova (2015), Tectonic evolution of the Mesozoic South Anyui suture zone, eastern Russia: A critical component of paleogeographic reconstructions of the Arctic region, *Geosphere,* 11(5), 1530-1564. https://doi.org/10.1130/GES01165.1

Amato, J. M., J. Toro, T. E. Moore, A. J. Sussman, and A. B. Weil (2004), Origin of the Bering Sea salient, in Orogenic curvature: Integrating paleomagnetic and structural analyses, In A. J. Sussman, Arlo, B, Weil (Eds), *Orogenic curvature: Integrating paleomagnetic and structural analyses* (Vol. 383, pp. 131-144), Geological Society of America. https://doi.org/10.1130/0-8137-2383-3(2004)383[131:ootbss]2.0.co;2

Andersen, O. B., Knudsen, P., & Berry, P. A. (2010). The DNSC08GRA global marine gravity field from double retracked satellite altimetry. Journal of Geodesy, 84(3), 191–199.

https://doi.org/10.1007/7s00190-009-0355-9

Bouligand, C., J. Dyment, Y. Gallet, and G. Hulot (2006), Geomagnetic field variations between chrons 33r and 19r (83–41 Ma) from sea-surface magnetic anomaly profiles, *Earth and Planetary Science Letters,* 250(3-4), 541-560. https://doi.org/10.1016/j.epsl.2006.06.051

Brune, S., C. Heine, M. Pérez-Gussinyé, and S. V. Sobolev (2014), Rift migration explains continental margin asymmetry and crustal hyper-extension, *Nature Communications,* 5, 4014.https://doi.org/10.1038/ncomms5014

Carey, S. W. (1955), The orocline concept in geotectonics-Part I, *Papers and proceedings of the Royal Society of Tasmania,* 80: 255-288.

Channell, J. E. T. (1995). Recalibration of the geomagnetic polarity timescale. Reviews of Geophysics, 33(S1), 161–168. https://doi.org/ 10.1029/95RG00404

Chian, D., H. R. Jackson, D. R. Hutchinson, J. W. Shimeld, G. N. Oakey, N. Lebedeva-Ivanova, Q. Li, R. W. Saltus, and D. C. Mosher (2016), Distribution of crustal types in Canada basin, Arctic Ocean, *Tectonophysics,* 691, 8-30. https://doi.org/10.1016/j.tecto.2016.01.038

Churkin, M., and J. H. Trexler (1981), Continental Plates and Accreted Oceanic Terranes in the Arctic, In A. E. M. Nairn, M. Churkin, F. G. Stehli (Eds.), *The Arctic Ocean* (pp. 1-20). US, Boston, MA: Springer. https://doi.org/10.1007/978-1-4757-1248-3_1

DeMets, C., R. G. Gordon, and D. F. Argus (2010), Geologically current plate motions, *Geophysical Journal International,* 181(1), 1-80. https://doi.org/10.1111/j.1365-246X.2009.04491.x

Dick, H. J., J. Lin, and H. Schouten (2003), An ultraslow-spreading class of ocean ridge, *Nature,* 426(6965), 405. https://doi.org/10.1038/nature02128

Døssing, A., Gaina, C., Andersen, O. B., & Jackson, R. (2018). New details on Cretaceous ocean formation in the High Arctic based on satellite gravity data. Paper presented at the International Conference on Arctic Margins (ICAM VIII) Abstracts, Stockholm, Sweden.

Døssing, A.,C. Gaina, J. M. Brozena (2017), Building and breaking a large igneous province: An example from the High Arctic. *Geophysical Research Letters*, 44(12), 6011- 6019. https://doi.org/10.1002/2016GL072420

Døssing, A., H. R. Jackson, J. Matzka, I. Einarsson, T. M. Rasmussen, A. V. Olesen, and J. Brozena (2013), On the origin of the Amerasia Basin and the High Arctic Large Igneous Province—results of new aeromagnetic data, *Earth and Planetary Science Letters,* 363, 219-230. https://doi.org/10.1016/j.epsl.2012.12.013

Embry, A. (2000), Counterclockwise rotation of the Arctic Alaska Plate: best available model or untenable hypothesis for the opening of the Amerasia Basin, *Polarforschung,* 68, 247-255.

Embry, A. F. (1990), Geological and geophysical evidence in support of the hypothesis of anticlockwise rotation of northern Alaska, *Marine Geology,* 93, 317-329. https://doi.org/10.1016/0025-3227(90)90090-7

Embry, A. F., and J. Dixon (1990), The breakup unconformity of the Amerasia Basin, Arctic Ocean: Evidence from Arctic Canada, *Geological Society of America Bulletin,* 102(11), 1526-1534. https://doi.org/10.1130/0016-7606(1990)102<1526:TBUOTA>2.3.CO;2

Franke, D. (2013). Rifting, lithosphere breakup and volcanism: Comparison of magma-poor and volcanic rifted margins. Marine and Petroleum Geology, 43, 63–87.

https://doi.org/10.1016/j.marpetgeo.2012.11.003

Gaina, C., Medvedev, S., Torsvik, T. H., Koulakov, I., & Werner, S. C. (2014). 4D Arctic: A glimpse into the structure and evolution of the Arctic in the light of new geophysical maps, plate tectonics and tomographic models. Surveys in Geophysics, 35(5), 1095–1122. https://doi.org/10.1007/s10712-013-9254-y

Gaina, C., Werner, S. C., Saltus, R., & Maus, S. (2011). Circum-Arctic mapping project: New magnetic and gravity anomaly maps of the Arctic. In A. M. Spencer, A. F. Embry, D. L. Gautier, A. V. Stoupakova, & K. Sørensen (Eds.), Arctic Petroleum Geology (Vol. 35, pp. 39–48). London: Geological Society of London. https://doi.org/10.1144/M35.3

Gee, J. S., and D. V. Kent (2007), Source of oceanic magnetic anomalies and the geomagnetic polarity time scale, In M. Kono (Ed), *Treatise on Geophysics: Geomagnetism*(Vol. 5, pp. 455-507).Elsevier. https://doi.org/10.1016/B978-044452748-6/00097-3

Granot, R., Dyment, J., & Gallet, Y. (2012). Geomagnetic field variability during the Cretaceous Normal Superchron. Nature Geoscience, 5(3), 220–223. https://doi.org/10.1038/NGEO1404

Grantz, A., D. Clark, R. Phillips, S. Srivastava, C. Blome, L. Gray, H. Haga, B. Mamet, D. McIntyre, and D. McNeil (1998), Phanerozoic stratigraphy of Northwind Ridge, magnetic anomalies in the Canada basin, and the geometry and timing of rifting in the Amerasia basin, Arctic Ocean, *Geological Society of America Bulletin,* 110(6), 801-820. https://doi.org/10.1130/0016-7606(1998)110<0801:psonrm>2.3.co;2

Grantz, A., P. E. Hart, V. A. Childers, A. M. Spencer, A. F. Embry, D. L. Gautier, A. V. Stoupakova, and K. Sørensen (2011), Geology and tectonic development of the Amerasia and Canada

Basins, Arctic Ocean, In A. M. Spencer, A. F. Embry, D. L. Gautier, A. V. Stoupakova, K. Sørensen(Eds.),*Arctic Petroleum Geology* (Vol. 35, pp.771-799), London: Geological Society of London. https://doi.org/10.1144/M35.50

Grantz, A., and S. D. May (1982), Rifting History and Structural Development of the Continental Margin North of Alaska, In J. S. Watkins, C. L. Drake (Eds.), *Studies in Continental Margin Geology* (Vol. 34, pp. 77-100), Tulsa,OK:American Association of Petroleum Geologists. https://doi.org/10.1306/M34430C4

Guspi, F. (1987), Frequency-domain reduction of potential field measurements to a horizontal plane, *Geoexploration,* 24(2), 87-98.https://doi.org/10.1016/0016-7142(87)90083-4

Halgedahl, S., and R. Jarrard (1987), Paleomagnetism of the Kuparuk River Formation from oriented drill core: Evidence for rotation of the Arctic Alaska plate,In: I. L. Tailleur, P. Weimer (Eds.) *Alaskan North Slope Geology* (Vol.2, pp. 581-617). Bakersfield, CA: Pacific Section, Society of Economic Paleontologists and Mineralogists.

Hubbard, R. J., S. P. Edrich, and R. P. Rattey (1987), Geologic evolution and hydrocarbon habitat of the ‘Arctic Alaska microplate’, *Marine and Petroleum Geology,* 4(1), 2-34. https://doi.org/10.1016/0264-8172(87)90019-5

Hutchinson, D. R., H. R. Jackson, D. W. Houseknecht, Q. Li, J. W. Shimeld, D. C. Mosher, D. Chian, R. W. Saltus, and G. N. Oakey (2017), Significance of Northeast‐Trending Features in Canada Basin, Arctic Ocean, *Geochemistry, Geophysics, Geosystems,* 18(11), 4156-4178. https://doi.org/10.1002/2017GC007099

Koulakov, I. Y., Gaina, C., Dobretsov, N., Vasilevsky, A., & Bushenkova, N. (2013). Plate reconstructions in the Arctic region based on joint analysis of gravity, magnetic, and seismic anomalies. Russian Geology and Geophysics, 54(8), 859–873. https://doi.org/10.1016/j.rgg.2013.07.007

Kuzmichev, A. B. (2009). Where does the South Anyui suture go in the New Siberian islands and Laptev Sea?: Implications for the Amerasia basin origin. Tectonophysics, 463(1), 86–108. https://doi.org/10.1016/j.tecto.2008.09.017

Lane, L. S. (1997), Canada Basin, Arctic Ocean: evidence against a rotational origin, *Tectonics,* 16(3), 363-387. https://doi.org/10.1029/97tc00432

Langseth, M. (1990), Geothermal observations in the Arctic region, In A. Grantz, G. L. Johnson, J. F. Sweeney, (Eds), *The Arctic Ocean Region* (pp. 133–151). Boulder, CO: Geological Society of America. https://doi.org/10.1130/DNAG-GNA-L.133

Lawver, L., and C. Scotese (1990), A review of tectonic models for the evolution of the Canada Basin, In A. Grantz, G. L. Johnson, J. F. Sweeney, (Eds), *The Arctic Ocean Region* (pp. 593–618). Boulder, CO: Geological Society of America. https://doi.org/10.1130/DNAG-GNA-L.593

Layer, P. W., R. Newberry, K. Fujita, L. Parfenov, V. Trunilina, and A. Bakharev (2001), Tectonic setting of the plutonic belts of Yakutia, northeast Russia, based on 40Ar/39Ar geochronology and trace element geochemistry, *Geology,* 29(2), 167-170. https://doi.org/10.1130/0091-7613(2001)029<0167:tsotpb>2.0.co;2

Malinverno, A. (1991), Inverse square-root dependence of mid-ocean-ridge flank roughness on spreading rate, *Nature,* 352(6330), 58. https://doi.org/10.1038/352058a0

Malinverno, A., J. Hildebrandt, M. Tominaga, and J. E. Channell (2012), M‐sequence geomagnetic polarity time scale (MHTC12) that steadies global spreading rates and incorporates astrochronology constraints, *Journal of Geophysical Research,* 117(B6). https://doi.org/10.1029/2012JB009260

Mickey, M. B., A. Bymes, and H. Haga (2002), Biostratigraphic evidence for the prerift position of the North Slope, Alaska, and Arctic Islands, Canada, and Sinemurian incipient rifting of the Canada Basin,In E. L.Miller, A.Grantz, S. L.Klemperer(Eds), *Tectonic Evolution of the Bering–Chukchi Sea–ArcticMargin and Adjacent Landmasses* (Vol. 60, pp. 67-76). Boulder, CO: Geological Society of America. https://doi.org/10.1130/0-8137-2360-4.67

Miller, E., S. Katkov, A. Strickland, J. Toro, V. Akinin, and T. Dumitru (2009), Geochronology and thermochronology of Cretaceous plutons and metamorphic country rocks, Anyui-Chukotka fold belt, North East Arctic Russia,In: D.B.Stone, K.Fujita, P.L.Layer, E.L.Miller, A.V. Prokopiev,J.Toro(Eds), *Geology, Geophysics and Tectonics of Northeastern Russia: a Tribute to Leonid Parfenov*(Vol. 4, pp. 223-241).Copernicus, Göttingen: European Geosciences Union. https://doi.org/10.5194/smsps-4-157-2009

Miller, E. L., K. E. Meisling, V. V. Akinin, K. Brumley, B. J. Coakley, E. S. Gottlieb, C. W. Hoiland, T. M. O'Brien, A. Soboleva, and J. Toro (2017), Circum-Arctic Lithosphere Evolution (CALE) Transect C: displacement of the Arctic Alaska–Chukotka microplate towards the Pacific during opening of the Amerasia Basin of the Arctic, In V. Pease,B. Coakle (Eds), *Circum-Arctic Lithosphere Evolution* (Vol. 460, pp. 57-120), London: Geological Society, London. https://doi.org/10.1144/SP460.9

Miller, E. L., J. Toro, G. Gehrels, J. M. Amato, A. Prokopiev, M. I. Tuchkova, V. V. Akinin, T. A. Dumitru, T. E. Moore, and M. P. Cecile (2006), New insights into Arctic paleogeography and tectonics from U‐Pb detrital zircon geochronology, *Tectonics,* 25, TC3013. https://doi.org/10.1029/2005TC001830

Miller, S. P. (1977), The validity of the geological interpretations of marine magnetic anomalies, *Geophysical Journal of the Royal Astronomical Society,* 50(1), 1-21. https://doi.org/10.1111/j.1365-246x.1977.tb01320.x

Mosher, D. C., and D. R. Hutchinson (2019), Canada Basin, In A. Piskarev, V. Poselov, V, Kaminsky (Eds.), *Geologic Structures of the Arctic Basin (*pp. 295-325*)*, Springer. https://doi.org/10.1007/978-3-319-77742-9_10

Müller, R. D., M. Seton, S. Zahirovic, S. E. Williams, K. J. Matthews, N. M. Wright, G. E. Shephard, K. T. Maloney, N. Barnett-Moore, and M. Hosseinpour (2016), Ocean basin evolution and global-scale plate reorganization events since Pangea breakup, *Annual Review of Earth and Planetary Sciences,* 44, 107-138. https://doi.org/10.1146/annurev-earth-060115-012211

Nokleberg, W. J. (2000), Phanerozoic tectonic evolution of the Circum-North Pacific, US Department of the Interior, US Geological Survey Open File Report, 98-754. https://doi.org/10.3133/pp1626

Ogg, J. (2012), Geomagnetic polarity time scale, In F. M. Gradstein, J. G. Ogg, M. D. Schmitz, G. M. Ogg (Eds), *The Geologic Time Scale* (pp. 85-113). Elsevier. https://doi.org/10.1016/B978-0-444-59425-9.00005-6

Sandwell, D. T., R. D. Müller, W. H. Smith, E. Garcia, and R. Francis (2014), New global marine gravity model from CryoSat-2 and Jason-1 reveals buried tectonic structure, *Science,* 346(6205), 65-67. https://doi.org/10.1126/science.1258213

Seton, M., R. Müller, S. Zahirovic, C. Gaina, T. Torsvik, G. Shephard, A. Talsma, M. Gurnis, M. Turner, and S. Maus (2012), Global continental and ocean basin reconstructions since 200 Ma, *Earth-Science Reviews,* 113(3-4), 212-270. https://doi.org/10.1016/j.earscirev.2012.03.002

Shephard, G. E., R. D. Müller, and M. Seton (2013), The tectonic evolution of the Arctic since Pangea breakup: Integrating constraints from surface geology and geophysics with mantle structure, *Earth-Science Reviews,* 124, 148-183. https://doi.org/10.1016/j.earscirev.2013.05.012

Sokolov, S., G. Y. Bondarenko, P. Layer, and I. Kravchenko-Berezhnoy (2009), South Anyui suture: tectono-stratigraphy, deformations, and principal tectonic events, *Stephan Mueller Special Publication Series,* 4, 201-221. https://doi.org/10.5194/smsps-4-201-2009

Sokolov, S. D., G. Y. Bondarenko, O. L. Morozov, V. A. Shekhovtsov, S. P. Glotov, A. V. Ganelin, and I. R. Kravchenko-Berezhnoy (2002), South Anyui suture, northeast Arctic Russia: facts and problems, In E. L. Miller, A. Grantz, S. L. Klemperer (Eds.) *Tectonic Evolution of the Bering Shelf-Chukchi Sea-Artic Margin and Adjacent Landmasses* (Vol. 360, pp. 209-224), Geological society of America. https://doi.org/10.1130/0-8137-2360-4.209

Taylor, P., L. Kovacs, P. Vogt, and G. Johnson (1981), Detailed aeromagnetic investigation of the Arctic Basin: 2, *Journal of Geophysical Research,* 86(B7), 6323-6333.

https://doi.org/10.1029/JB086iB07p06323

Thébault, E., C. C. Finlay, P. Alken, C. D. Beggan, E. Canet, A. Chulliat, B. Langlais, V. Lesur, F. J. Lowes, and C. Manoj (2015), Evaluation of candidate geomagnetic field models for IGRF-12, *Earth, Planets and Space,* 67(1), 112. https://doi.org/10.5047/eps.2010.11.005

Toksöz, M. N., & Hsui, A. T. (1978). Numerical studies of back-arc convection and the formation of marginal basins. Tectonophysics, 50(2-3), 177–196. https://doi.org/10.1016/0040-1951(78)90134-8

Toro, J., Amato, J. M., & Natal'in, B. (2003). Cretaceous deformation, Chegitun River area, Chukotka Peninsula, Russia: Implications for the tectonic evolution of the Bering Strait region. Tectonics, 22(3), 1021. https://doi.org/10.1029/2001TC001333

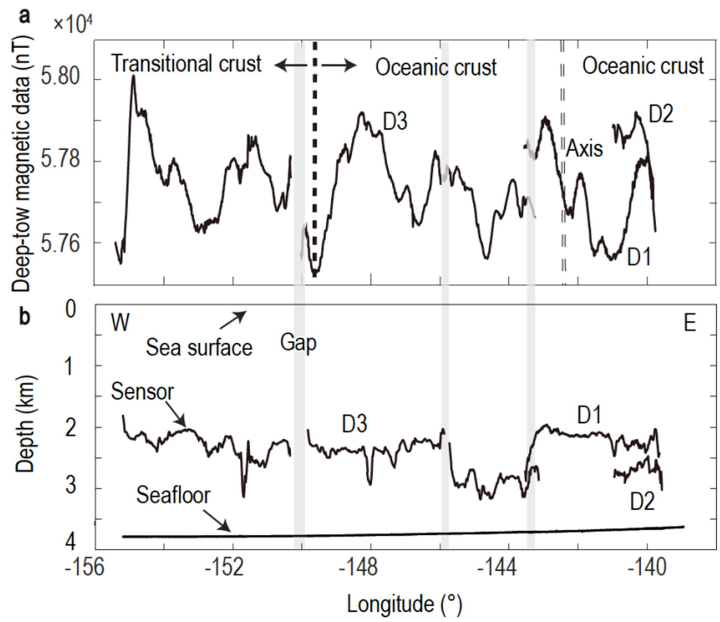

Figure S1. Raw deep-tow magnetic data (a) and depth of the sensor (b). The near E-W trending deep-tow magnetic profile consists of three sections (D1-D3). Section D1 is along ~76.07°N and is located ~40 km north of the other sections.

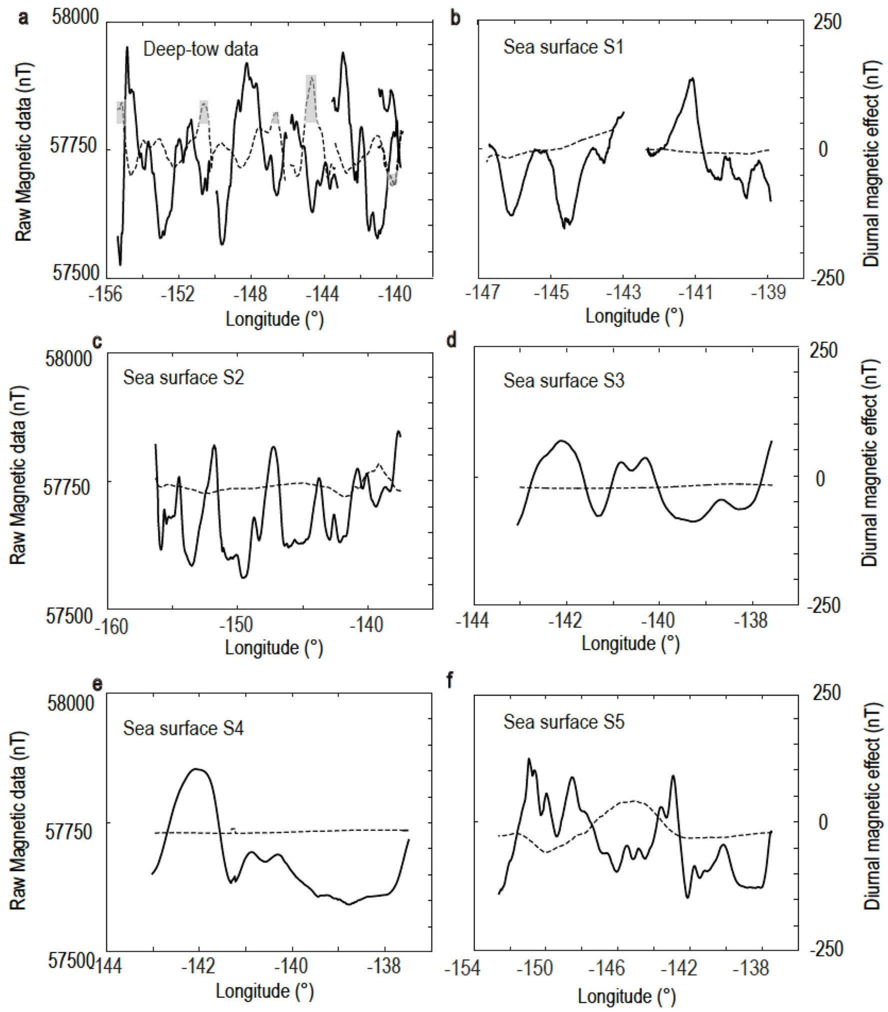

Figure S2. Comparisons between the raw magnetic data (solid lines) and the diurnal effects (dashed lines).The STD of the diurnal variation for the sea surface surveys in 2016 and 2017 is 11.3 nT and 14.3 nT, respectively. The diurnal variations with amplitudes > 50 nT are covered with gray boxes.

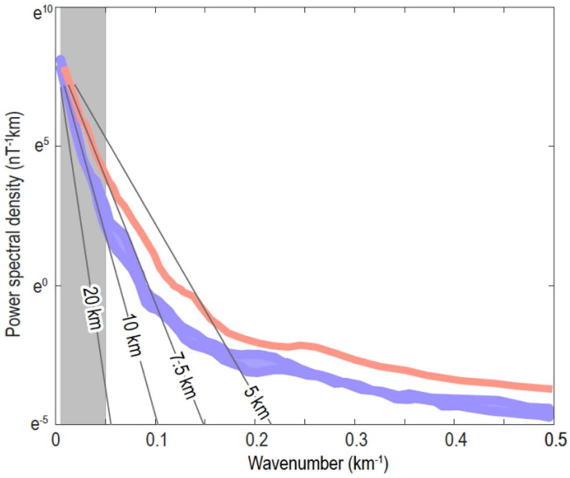

Figure S3. Power spectral densities computed from the sea surface (blue) and deep-tow upward continued to sea surface data (red). The blue shaded area represents variance. The gray shaded area indicates thesignals with wavelengths between 20 km and 300 km, which is most likely due to crustal sources.

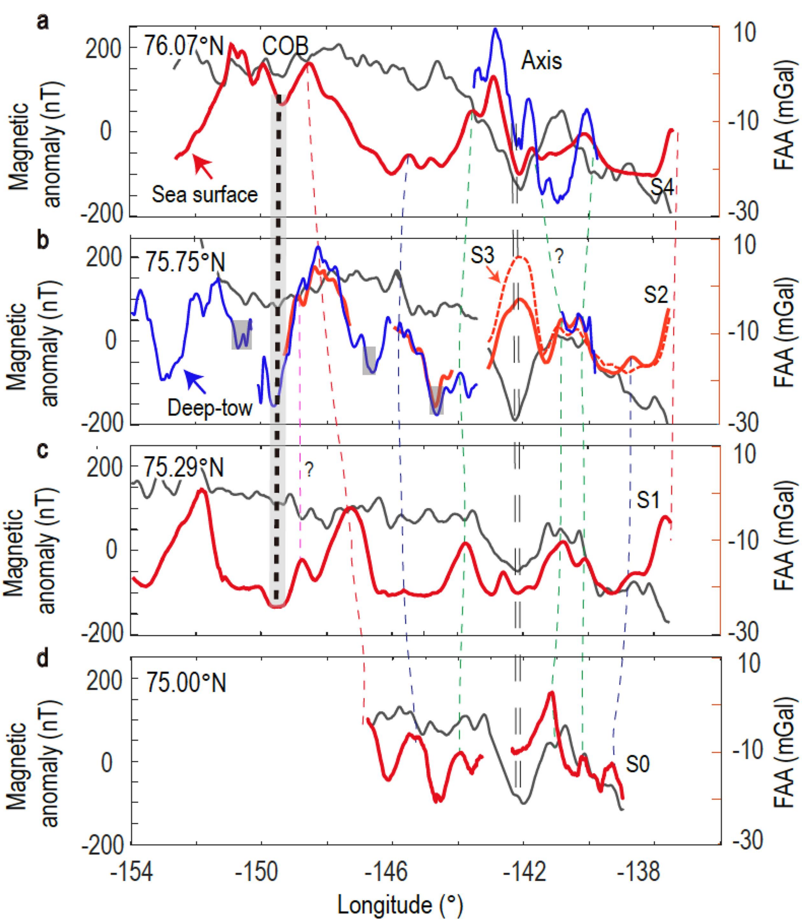

Figure S4. Free air anomaly (FAA) along the tracks of magnetic data. The FAA data (black lines) are from *Sandwell et al.* [2014]. Note that the two broad magnetic highs (N1 and N2) are not correlated with the FAA.

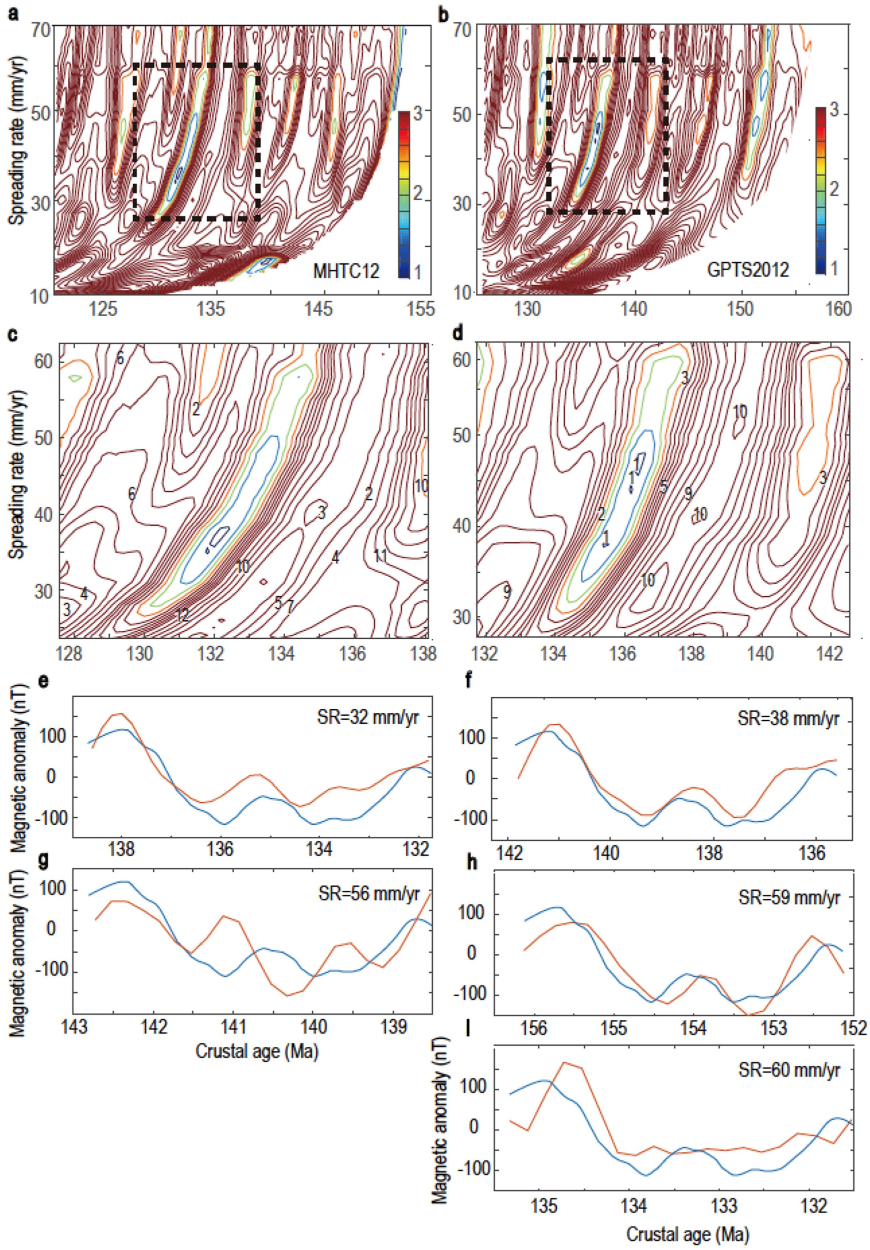

Figure S5. Estimation procedure of the best fit sequences. (a-b) Contours of the least-squares misfit of the anomaly between the characteristic stacked data and synthetic data based on

MHTC12 (a) and GTS2012 (b). The cross-correlation method compares the stacked and synthetic data based on least-squares fitting criteria [*DeMets et al.,* 2010]. In each comparison, the amplitude scale of the synthetic data is adjusted to match the peak-to-trough amplitude of N1 and N2. The contours are normalized by the misfit of the best-fitting least-squares model. **(**c-d**)** The contours around the best-fitting model in the dashed frames of (a-b). (e-f) Comparison of the stacked data and best-fitting data based on MHTC12 (e) and GTS2012 (f). (g-i) Comparison of the stacked data and other candidates of the best-fitting models based on MHTC12 (g) and GTS2012 (h and i). The spreading rates (SR) are also shown.

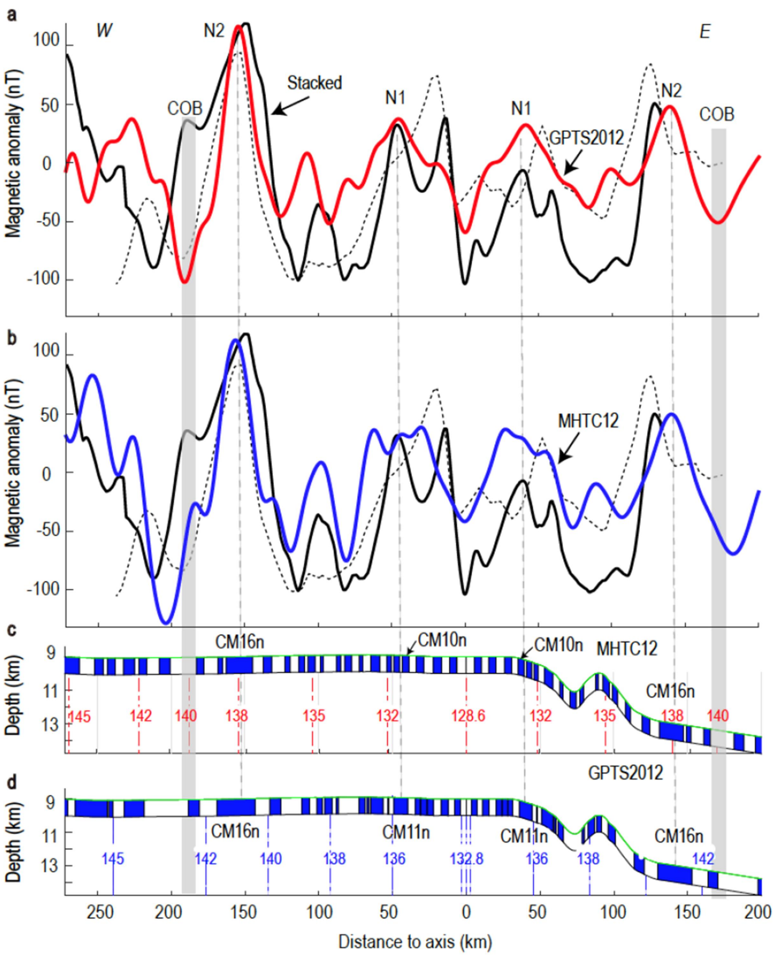

Figure S6. Identification of the crustal age in the Canada Basin. (a-b) Comparison between the stacked magnetic anomalies (black lines) and the best-fitting synthetic magnetic anomalies. The synthetic magnetic anomalies produced by the magnetic bodies in MHTC12 and GTS2012 are shown in red and blue, respectively. Stacked airborne magnetic anomaly is also shown (dashed line). (c-d) The best-fitting magnetic sequences in MHTC12 (c) and GTS2012 (d).